Sharpening the shape distribution of gold nanoparticles by laser irradiation

V. Resta, J. Siegel, J. Bonse, J. Gonzalo, C. N. Afonso et al.

Citation: J. Appl. Phys. **100**, 084311 (2006); doi: 10.1063/1.2358822
View online: http://dx.doi.org/10.1063/1.2358822
View Table of Contents: http://jap.aip.org/resource/1/JAPIAU/v100/i8
Published by the American Institute of Physics.

Sharpening the shape distribution of gold nanoparticles by laser irradiation

V. Resta,[a] J. Siegel, J. Bonse, J. Gonzalo, and C. N. Afonso
Laser Processing Group, Instituto de Óptica, CSIC, Serrano 121, E-28006 Madrid, Spain

E. Piscopiello and G. Van Tenedeloo
EMAT, University of Antwerp, Groenenborgerlaan 171, B-2020 Antwerp, Belgium

(Received 16 May 2006; accepted 24 July 2006; published online 19 October 2006)

This work reports on the optical response and morphological changes of gold nanoparticles (NPs) induced by laser irradiation with single nanosecond laser pulses of different fluences and wavelengths. The as-grown specimens consist of irregularly shaped NPs (10–13 nm in average dimensions) produced by pulsed laser deposition on a substrate. They exhibit a broad optical absorption band related to the surface plasmon resonance (SPR) peaking in the range of 634–685 nm. After irradiation with fluences above a threshold value, a blueshift, a decrease of the overall absorption, and a narrowing of the SPR band are observed. The SPR peak wavelength and amplitude after irradiation at increasing fluences reach an approximately constant value, irrespective of the irradiation wavelength. This value is consistent with a homogeneous distribution of spherical gold NPs with a mean diameter close to the average initial dimensions as determined by transmission electron microscopy. The results demonstrate that the conversion of irregularly shaped NPs into spherical NPs with reduced dimension dispersion is a thermally driven process and occurs within a fluence interval defined by the melting threshold of *all* NPs and the ablation threshold. Whereas the useful fluence interval is controlled by the effective fluence absorbed, that is dependent on the laser wavelength and thermal properties of the substrate, the final shape and dimensions of the NPs are independent of the irradiation wavelength provided the fluence is within this useful interval. © *2006 American Institute of Physics*. [DOI: 10.1063/1.2358822]

INTRODUCTION

Nanoparticles (NPs) are the subject of renewed interest in part because they can be used as building blocks for the formation of nanostructured materials with possible applications in fields ranging from information-related applications, such as data storage or all-optical switching, to different types of sensors for environment, medical, or biological applications. Since the properties of NPs depend on their dimensions, shape, and surrounding media, irrespective of whether the NPs are on surfaces or dissolved/embedded in media, it is of primary importance to develop techniques able to achieve low dimension and shape dispersion.

The optical response of metal NPs is characterized by an absorption band related to the surface plasmon resonance (SPR).[1–3] Laser irradiation with nanosecond pulses or shorter at wavelengths within this band thus provides a means for selectively heating NPs while keeping the surrounding nonabsorbing media cool. This approach has widely been used in the case of noble metals to change both dimensions and shape of NPs via melting and evaporation.[1,4] Whereas laser irradiation of NPs dissolved in liquids often leads to a reduction of dimensions[5] or fragmentation,[6] the most widely reported result when irradiating NPs on substrates is the conversion of irregular NPs or islands into spherical NPs.[7–10] Furthermore, colloidal gold nanorods are converted into spherical NPs after irradiation with laser pulses, the efficiency of the process being higher for femtosecond than for nanosecond laser pulses and independent of the excitation wavelength.[1,4] These results are in contrast to the control of the aspect ratio by changing the wavelength reported for silver NPs.[11]

A case material for most of these studies has been Au, most likely because the SPR of Au NPs can be tuned from the visible to the near IR range of the spectrum by changing the dimensions, shape, or surrounding media. This is different for Ag, for which the SPR can also be tuned but in a range shifted to the near UV. Most of the work reported on laser irradiation of Au NPs on surfaces[8–10] uses a single wavelength much shorter (248 and 355 nm) than that of the SPR of spherical Au NPs (typically around 530 nm).[2] At those short irradiation wavelengths, the absorption is dominated by interband transitions that may screen the possible size selectivity effect from resonant plasmon excitation reported elsewhere for the case of Ag NPs during growth.[11] In addition, a single laser fluence is used in most cases,[7–10] and the results relate to large NPs (>35 nm)[7,8,10] for which the melting temperature is expected to be close to that of the bulk material.[12]

The aim of this work is to determine the role of laser fluence and wavelength in sharpening the dimension and shape distributions of irregularly shaped NPs on substrates by laser irradiation. The NPs studied in this work are produced by pulsed laser deposition (PLD) and thus by nucleation and diffusion at the substrate following the Volmer-Weber growth.[13] This method leads to sharp distributions of quasispherical NPs for low metal contents ($\leqslant 5 \times 10^{15}$ at. cm^{-2}) and to irregularly shaped NPs due to coars-

[a]Author to whom correspondence should be addressed; FAX: +34-91-5645557; electronic mail: v.resta@io.cfmac.csic.es

ening and coalescence for higher values ($\geqslant 6 \times 10^{15}$ at. cm^{-2}).[14,15] In this work, we have selected the latter type of NPs with average dimensions of 10–13 nm and we have used irradiation wavelengths up to that of the SPR peak in order to explore the possibility of tailoring the NP dimensions and shape through the laser irradiation wavelength as suggested elsewhere.[11]

EXPERIMENT

The samples were produced by PLD in vacuum (5×10^{-6} mbar) on glass and carbon-coated mica (C-mica) substrates held at room temperature. The substrates were placed in front of the target and rotated in order to obtain a homogeneously thick specimen (within 5%) in an area >150 mm^2. A 10 nm layer of amorphous Al_2O_3 was first deposited in order to have the NPs always nucleated on the same surface and irrespective of the substrate used. The specimens have been produced by focusing an ArF laser beam [$\lambda = 193$ nm, $\tau = 20$ ns full width half maximum (FWHM)] alternatively on Al_2O_3 and Au targets at an angle of 45° with respect to the target normal. The laser repetition rate was set at 20 Hz and the fluence at the target site was ~ 2.7 J cm^{-2}. Further details on the deposition procedure on static substrates can be found elsewhere.[14]

After deposition, the specimens have been irradiated in air using single ~6 ns pulses from a tunable optical parametric oscillator (Spectra Physics, MOPO-HF) pumped by the third harmonic of a Nd:YAG (yttrium aluminum garnet) laser (Spectra Physics Quanta-Ray PRO-250) at several wavelengths in the range of 470–650 nm. A beam homogenizer has been used to obtain a homogeneous top-hat intensity profile at the sample site with constant laser energy over a square region of 2.5×2.5 mm^2. After each laser pulse, the sample was translated to expose a new fresh area to the next pulse. The optical extinction spectra of the specimens are determined from the experimentally measured transmission (T) spectra as $\ln(1/T)$. The latter were measured *ex situ* using a spectroscopic ellipsometer (WVASE) in the range of 350–850 nm. Since measurements at different angles of incidence (0°, 25°, 45°, 65°) and both p and s polarizations showed no significant differences, all results reported in this work have been obtained at 0° of incidence angle with polarized light. The changes induced in the neighborhood of the SPR by laser irradiation were also evaluated *in situ* by measuring the transmission spectrum of the specimen at normal incidence before and after irradiation using an unpolarized beam from a Hg–Xe lamp as illumination source and a fiber-coupled spectrometer (CVI-SM-240) as detector.

Both as-grown and laser irradiated areas of specimens deposited on C-mica substrates were floated off the mica substrate in distilled water and collected on transmission electron microscope (TEM) grids. The NP features have been determined by imaging these specimens in a JEOL 4000EX (400 kV) TEM with 0.17 nm point-to-point resolution. The analysis of the images was performed by manually outlining the NP boundaries contained in an area of at least 200×200 nm^2 in order to convert them into binary images from which the dimensions of NPs were determined.

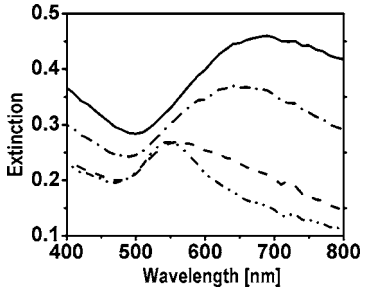

FIG. 1. Extinction spectra determined from *ex situ* optical measurements from (solid line) as-grown and laser irradiated areas at 530 nm with (dash-dotted line) 49 mJ cm^{-2}, (dashed line), 94 mJ cm^{-2}, and (dash-double dotted line) 136 mJ cm^{-2}. The specimen has been produced on glass substrate.

A selection of as-grown and irradiated areas of specimens deposited on glass substrates was analyzed by Rutherford backscattering (RBS) using a 3 MeV proton beam. The results show that both as-grown and irradiated areas have on average 13×10^{15} at. cm^{-2} of Au (within 8%). For very large laser fluences (depending on substrate and wavelength), a reduction of the Au content with respect to the as-grown specimen is in some cases observed, most likely due to evaporation/ablation. In the following, only results related to fluences below this threshold are presented.

RESULTS

Figure 1 shows the *ex situ* measured optical extinction spectra of a selection of as-grown and laser irradiated areas of a specimen deposited on glass substrate. The as-grown area shows a broad absorption band related to the SPR peaking at 685 nm. The spectra of areas irradiated at a wavelength of 530 nm and low fluence (see spectrum obtained for 49 mJ cm^{-2}) show an overall lower absorption amplitude and a SPR shifted to shorter wavelengths. At higher fluences (see spectra obtained for $\geqslant 94$ mJ cm^{-2}), a significant narrowing of the SPR and a strong reduction of the absorption in the near IR are observed. These changes are seen in a quantitative way in Fig. 2 where the peak wavelength, extinction, and width of the SPR are plotted as a function of the irradiation fluence. In spite of the fact that these three magnitudes decrease as fluence increases, there is a noticeable difference between them: whereas the width [Fig. 2(c)] follows a quasi-monotonous decrease, the peak wavelength and extinction [Figs. 2(a) and 2(b)] follow a saturation-like behavior that can be appreciated for fluences above ≈ 90 mJ cm^{-2}, when both magnitudes reach an approximately constant value.

Figure 3 shows the wavelength of the SPR peak determined from *in situ* measurements after irradiation at 530 nm as a function of laser fluence for specimens grown on C-mica and glass substrates produced in the same deposition run. As in the case of Fig. 2, the values plotted at zero fluence refer to the as-grown specimens and they show that both films exhibit the same SPR peak position, confirming both specimens have NPs with similar features. The figure also includes results for a different specimen on C-mica substrate that has initially slightly smaller or more spherical NPs as evidenced by the fact that the SPR peak in the as-grown specimen appears at slightly shorter wavelength. The speci-

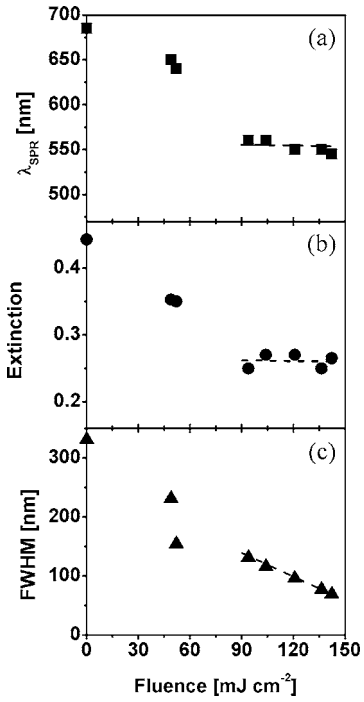

FIG. 2. (a) Peak wavelength, (b) extinction, and (c) FWHM of SPR determined from *ex situ* optical measurements as a function of the laser fluence used to irradiate at 530 nm a specimen produced on glass substrate. The values at zero fluence correspond to the as-grown specimen.

men on glass is the specimen in which the results plotted in Figs. 1 and 2 are obtained. The comparison of Figs. 2 and 3 evidences the agreement between results from *in situ* and *ex situ* experiments. The spread of the data observed in Fig. 3 for specimens on C-mica substrates is most likely related to inhomogeneities of the carbon deposit. Within this dispersion, the evolution of the SPR peak as a function of irradiation fluence in the two specimens on C-mica substrates is very similar irrespective of the initial wavelength of the SPR peak. The overall evolution of the SPR peak in specimens on C-mica substrates is also similar to the one observed on glass, the only remarkable difference being the fact that the blueshift of the SPR peak for specimens on C-mica substrates occurs at lower fluences. Consistently, the ablation threshold for specimens on C-mica substrates is also lower and thus, the interval of useful fluences is narrower and shifted to lower values in this case. This interpretation is based on the observation of a reduction of metal when irradiating films on C-mica substrates at 530 nm with fluences $\geqslant$65 mJ cm^{-2} whereas no such reduction is observed at the same wavelength for films on glass substrates up to the highest fluence used (168 mJ cm^{-2}).

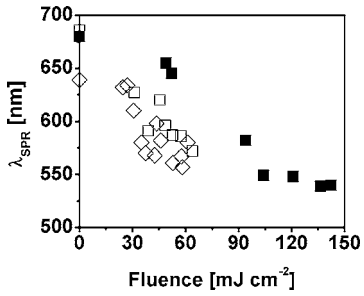

FIG. 3. Peak wavelength of SPR determined from *in situ* optical measurements as a function of the laser fluence used to irradiate at 530 nm specimens on (■) glass and (□, ◇) C-mica substrates. The values at zero fluence correspond to the as-grown specimens.

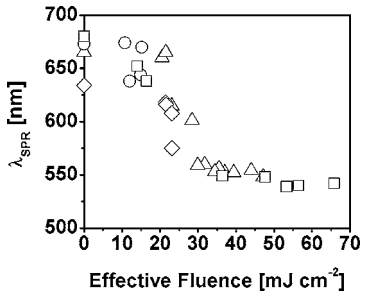

FIG. 4. Peak wavelength of SPR determined from *in situ* optical measurements in laser irradiated areas as a function of the effective laser fluence used to irradiate specimens on glass substrates at several wavelengths: (○) 470 nm, (□) 530 nm, (△) 610 nm, and (◇) 650 nm. The values at zero fluence correspond to the as-grown specimen.

In order to take into account the different absorptions of the specimens at different laser wavelengths and thus use a parameter that directly relates to the temperature increase eventually achieved, we have defined the effective fluence as the irradiation fluence multiplied by the average value of the extinction coefficient of the as-grown specimen at the irradiation wavelength. Figure 4 shows the wavelength of the SPR peak as a function of this effective fluence after irradiating a specimen on glass substrate at several different wavelengths in the range of 470–650 nm. Both the extinction before irradiation and the SPR wavelength peak after irradiation are determined from *in situ* transmission measurements and all the as-grown areas had a SPR peaking in the 634–685 nm range. Similar results have been achieved in the specimens on C-mica although with a higher dispersion due to the inhomogeneities in the carbon coating. The combination of higher specimen absorption and higher output of the irradiation laser in the range of 530–610 nm results that the whole fluence interval could only be covered for these wavelengths. The results show that irrespective of the laser wavelength and the initial position of the SPR peak, the blueshift of the SPR after irradiation increases continuously with effective fluences in the range of 10–35 mJ cm^{-2}. For higher fluences, it remains approximately constant and close to 530 nm.

Figure 5 shows representative TEM images of an as-grown area [Fig. 5(a)] and three areas after laser irradiation [Figs. 5(b)–5(d)], corresponding to the specimen on C-mica whose optical data after irradiation are plotted in Fig. 3 and exhibits the shortest SPR peak wavelength before irradiation. The as-grown area [Fig. 5(a)] shows irregularly shaped and large NPs, many of them elongated due to coalescence. The area irradiated at the highest laser fluence [61 mJ cm^{-2} at 530 nm in Fig. 5(c)] only shows round NPs. The areas irradiated at intermediate fluences show either irregularly shaped NPs along with some round NPs [35 mJ cm^{-2} at 530 nm in Fig. 5(b)] or mostly round NPs with some irregularly shaped ones [32 mJ cm^{-2} at 610 nm in Fig. 5(d)]. In spite of using slightly lower fluence, the fraction of round NPs is higher in the area irradiated at 610 nm [Fig. 5(d)] than in the one

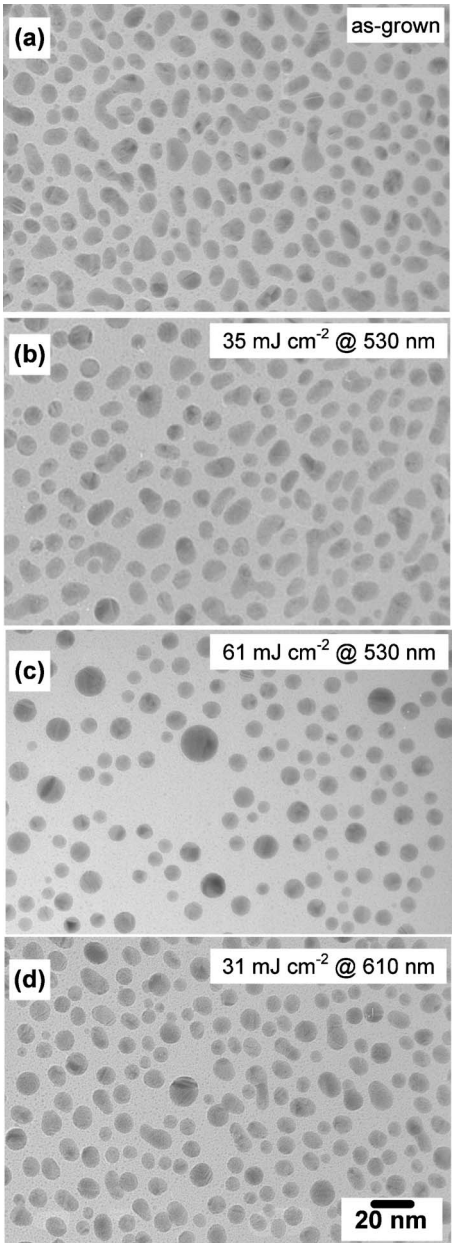

FIG. 5. TEM images of (a) as-grown and [(b)–(d)] laser irradiated areas. The laser wavelength and fluence are indicated in each image.

irradiated at 530 nm [Fig. 5(b)]. However, the effective fluence is higher in the former than in the latter case. This result together with those shown in Fig. 4 thus evidences that the conversion of irregularly shaped NPs to round ones scales with the effective fluence irrespective of the irradiation wavelength.

The in-plane NP dimensions have been determined from images in Fig. 5 by defining for each NP a length l (the longer dimension) and a width w (the in-plane dimension in the direction perpendicular to the length) and averaging data of more than 100 NPs. The results are summarized in Table I. The in-plane aspect ratio is calculated as l/w and is 1.38 in the as-grown area. After laser irradiation, the in-plane aspect ratio decreases and the dimension dispersion and the number density of NPs are reduced as the small NPs preferentially disappear. For the highest fluence, all NPs are round (aspect ratio of 1.0) and the diameter dispersion is very small. It is worth noting that this laser fluence is close to the one producing the highest SPR shift in Fig. 3 for specimens on C-mica substrates.

TABLE I. NP dimensions determined by TEM (Fig. 5) from as-grown and laser irradiated (LI) areas at a wavelength λ, where l and w are, respectively, the in-plane length and width of NPs, l/w is the aspect ratio, and N is the NP number density. The data are obtained by averaging values over 100 NPs and the errors are the dispersion of the data.

Area	λ (nm)	Fluence (mJ cm^{-2})	Effective fluence (mJ cm^{-2})	l (nm)	w (nm)	l/w	N ($\times 10^{11}$ cm^{-2})
As-grown	···	···	···	11±4	8±1	1.38	6
LI	530	35	8	11±2	9±1	1.22	6
LI	530	61	17	9±2	9±2	1.00	3
LI	610	32	11	10±2	9±2	1.11	5

DISCUSSION

The results obtained in this work show that three fluence regimes can be identified: (1) a low fluence regime where no significant changes are observed, (2) an intermediate fluence interval where the SPR continuously shifts to shorter wavelengths as fluence is increased, and (3) a high fluence regime where the SPR remains approximately constant. The boundary between regimes for the specimen on glass (Fig. 4) occurs at effective fluences of ≈10–15 mJ cm^{-2} and ≈30–35 mJ cm^{-2} and these boundaries generally depend on the thermal response of the system (Fig. 3) that in our case is mostly controlled by the thermal properties of the substrate. Once the fluence is above the threshold for transformation, round NPs start to appear. The number of round NPs is larger the higher the fluence within regime 2 [Figs. 5(b)–5(d)], thus leading to a continuous decrease of the NP in-plane aspect ratio within this regime.

A similar fluence dependence of the evolution of NP features has been reported elsewhere for NPs of very different initial features and irradiation conditions.[7,10] In the case of Au and Ag islands produced by sputtering on a substrate,[7] thus having similar features to the ones studied in this work, the conversion of irregularly shaped NPs into spherical ones upon laser irradiation at 532 nm occurs in a narrow fluence interval (our fluence regime 3) that has been related to laser-induced melting. A similar shape conversion is reported after irradiation of much larger NPs (38 nm of average major axis) at shorter wavelength (355 nm) and picosecond laser pulses.[10] These results further support the idea that the morphological transformations depend neither on the irradiation wavelength nor on the starting dimensions of the NPs. This conclusion is also in agreement with results achieved after irradiation of colloidal Au nanorods with both nanosecond and femtosecond laser pulses.[1,4] It is worth pointing out that most of the work reported in the literature on laser irradiation of metal NPs does not report the beam profile used.[7,8,10] The top-hat profile used in this work guarantees that the laser fluence is constant over the entire irradiated area. This is particularly important when measuring the optical spectra of the irradiated area using a white light source in order to

prevent averaging of the optical response of areas having a different degree of transformation or even no transformation.

In our case, the conversion of irregularly shaped NPs into round ones occurs along with the preferential disappearance of smaller NPs. A similar process has earlier been observed when irradiating large triangular Au NPs.[8] In that case, the first pulses lead to the formation of small NPs at the corners of the triangles, which disappear when the number of pulses was increased and the NPs became spherical. The round morphology of NPs after irradiation is consistent with melting followed by rapid solidification due to the cold substrate acting as an efficient heat sink. Since shape changes have a higher impact on the blueshift of the SPR peak than small changes in the average dimensions,[2] the SPR peak shifts observed in Figs. 2–4 within regime 2 are most likely dominated by the partial conversion of irregularly shaped NPs into round ones, in agreement with the TEM images in Fig. 5. The existence of a fluence interval in which this conversion is not complete can be understood by taking into account that the melting temperature of NPs is lower the smaller the NPs,[12] together with the fact that the smaller NPs possibly have lower evaporation/ablation coefficient and thus disappear first. This conclusion is further supported by the fact that *all* irradiation wavelengths studied lead to a single fluence regime 2 interval once the laser fluence has been converted into effective fluence (Fig. 4). Moreover, the shift of fluence regime 2 to lower fluences when changing the substrate (Fig. 3) further supports the thermal nature of the process. The thermal properties of the substrate control the thermal response of the specimen; the higher the thermal diffusivity, the lower the peak temperature and the faster the cooling rate. The thermal diffusivity of the substrates used has been calculated using the heat capacity, density, and thermal conductivity published elsewhere,[16] leading to a value for mica that is 0.6 times that of glass. However, this factor might be even lower due to the poor adhesion of the film to the C-mica substrate, effectively introducing an interface resistance. The peak temperature achieved when using the same fluence for specimens on C-mica substrates should thus be higher than that achieved on the same specimen on glass. The threshold fluence for producing changes is consequently lower and the fluence interval for complete transformation into round NPs should be narrower for specimens on C-mica as observed in Fig. 3. This reasoning is experimentally supported by the lower ablation threshold of the specimen on C-mica substrate that is at least a factor of 0.4 lower than that on glass.

At the limit between fluence regimes 2 and 3, most NPs become round [Fig. 5(c)] and this causes the wavelength and amplitude of the SPR peak to reach an approximately constant value. However, the width of the SPR remains decreasing as fluence is increased within regime 3 as seen in Fig. 1 (see spectrum obtained at 136 mJ cm^{-2}) and Fig. 2(c). Since the in-plane shape of NPs has become constant, the narrowing of the SPR as fluence is increased must be related to a further decrease of the dimension dispersion of the NPs while keeping constant the average dimension value. This can be explained by the fact that as fluence is increased, the substrate starts to be heated too and thus the cooling process slows down. Once this happens, the time the system stays molten becomes longer and thus longer diffusion lengths are achievable. This facilitates further coalescence of smaller NPs that contributes to decrease the dimension dispersion while keeping the average dimensions approximately constant. Besides, in the particular case of specimens studied in this work produced by PLD, it has been reported for several metals including Au that some metal ($<2\times10^{15}$ at. cm^{-2}) is implanted in the substrate (to a depth <2 nm) during the growth process in addition to the NPs formed at the surface.[14,15] The diffusion of implanted metal towards the surface and eventually reaching a NP can be promoted at high temperatures, thus providing a possible additional process contributing to regime 3.

Our experimental approach to determine the morphology of the NPs is based on plan view TEM observations and thus provides information on the dimensions of the NPs parallel to the substrate surface. The question whether the NPs are indeed spherical still remains, i.e., their height or dimension along the direction perpendicular to the substrate is similar to the in-plane dimensions. In the as-produced NPs, this height is most likely smaller than the average in-plane diameter according to earlier reports on different metallic NPs produced by alternate PLD under similar conditions.[13–15] However, this situation can change after laser-induced melting and solidification since these processes tend to reduce the surface energy and spheres are the most favorable geometry. This reasoning is consistent with the fact that while the average numbers of atoms determined by RBS and average in-plane dimensions do not change significantly upon irradiation, the number density is reduced. Therefore, the height of the NPs has to increase after irradiation and can approach that of spheres. Using the data in Table I for the highest fluence for which all NPs have converted into round NPs and assuming that the number of metal atoms remains approximately constant, the estimated height of the NPs after irradiation agrees with that of a sphere within the experimental error. Further support to this conclusion is the fact that both the shape and position of the SPR band within fluence regime 3 in Figs. 1–3 are very similar to the ones calculated for spherical NPs.[2]

CONCLUSIONS

Laser irradiation is a suitable tool for transforming irregularly shaped (10–13 nm average dimensions) gold nanoparticles on a substrate into spherical NPs with little dimension dispersion provided the fluence used is sufficiently high to melt *all* NPs. The transformation process is thermally driven and takes place in a useful fluence interval determined by this fluence and the ablation threshold. This interval depends on the thermal diffusivity of the substrate and shifts to lower values and narrows as the thermal diffusivity decreases. For fluences below the useful interval, the different absorptions and melting temperatures of NPs as a function of their morphology lead to preferential disappearance of small NPs and selective melting. The changes observed in the surface plasmon resonance are dominated by morphological changes as the NPs convert from irregularly shaped into

spherical ones rather than by significant variations in the average dimensions.

ACKNOWLEDGMENTS

The authors are grateful to Dr. J. García from Centro Nacional de Aceleradores (Spain) for performing the RBS measurements. This work has partially been supported by HPRN-CT-2002-00328, EU and MAT2005-06508-C02-01, MEC (Spain). One of the authors (J.B.) acknowledges the funding of the CSIC through a contract in the frame of the I3P program (Ref. No. I3P-Pc2002), cofunded by the European Social Fund.

[1]S. Link and M. A. El-Sayed, Int. Rev. Phys. Chem. **19**, 409 (2000) and references therein.
[2]L. M. Liz-Marzan, Langmuir **22**, 32 (2006).
[3]C. F. Bohren and D. R. Huffman, *Absorption and Scattering of Light by Small Particles* (Wiley, New York, 1983).
[4]S. Link and M. A. El-Sayed, Annu. Rev. Phys. Chem. **54**, 331 (2003) and references therein.
[5]H. Kurita, A. Takami, and S. Koda, Appl. Phys. Lett. **72**, 789 (1998).
[6]F. Mafune, Chem. Phys. Lett. **397**, 133 (2004).
[7]M. Kawasaki and M. Hori, J. Phys. Chem. B **107**, 6760 (2003).
[8]F. Sun, W. Cai, Y. Li, G. Duan, W. T. Nichols, C. Liang, N. Koshizaki, Q. Fang, and I. W. Boyd, Appl. Phys. B: Lasers Opt. **81**, 765 (2005).
[9]D.-Q. Yang, M. Meunier, and E. Sacher, J. Appl. Phys. **95**, 5023 (2004).
[10]S. Inasawa, M. Sugiyama, and Y. Yamaguchi, J. Phys. Chem. B **109**, 3104 (2005).
[11]F. Stietz, Appl. Phys. A: Mater. Sci. Process. **72**, 381 (2001).
[12]Ph. Buffat and J.-P. Borel, Phys. Rev. A **13**, 2287 (1976).
[13]R. Serna, C. N. Afonso, C. Ricolleau, Y. Wang, Y. Zheng, M. Gandais, and I. Vickridge, Appl. Phys. A: Mater. Sci. Process. **71**, 583 (2000).
[14]J. Gonzalo *et al.*, Phys. Rev. B **71**, 125420 (2005).
[15]J.-P. Barnes, A. K. Petford-Long, R. C. Doole, R. Serna, J. Gonzalo, A. Suarez-Garcia, C. N. Afonso, and D. Hole, Nanotechnology **13**, 465 (2002).
[16]*Handbook of Chemistry and Physics*, 82nd ed. (CRC, Boca Raton, FL, 2001); http://www.eriesci.com